

Chemically Cross-Linked Carbon Nanotube Films Engineered to Control Neuronal Signaling

Myriam Barrejón,^{†,⊥} Rossana Rauti,^{‡,⊥} Laura Ballerini,^{*,‡,⊥} and Maurizio Prato^{*,†,§,||}

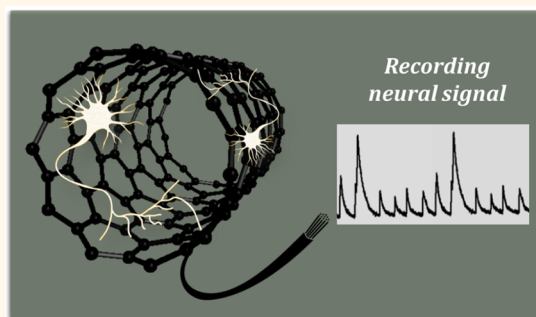
[†]Department of Chemical and Pharmaceutical Sciences, Università degli Studi di Trieste, Via Licio Giorgieri 1, Trieste 34127, Italy

[‡]International School for Advanced Studies (SISSA/ISAS), Trieste 34136, Italy

[§]Carbon Bionanotechnology Group, CIC biomaGUNE, Paseo Miramón 182, San Sebastián, Guipúzcoa 20014, Spain

^{||}Basque Foundation for Science, Ikerbasque, Bilbao 48013, Spain

ABSTRACT: In recent years, the use of free-standing carbon nanotube (CNT) films for neural tissue engineering has attracted tremendous attention. CNT films show large surface area and high electrical conductivity that combined with flexibility and biocompatibility may promote neuron growth and differentiation while stimulating neural activity. In addition, adhesion, survival, and growth of neurons can be modulated through chemical modification of CNTs. Axonal and synaptic signaling can also be positively tuned by these materials. Here we describe the ability of free-standing CNT films to influence neuronal activity. We demonstrate that the degree of cross-linking between the CNTs has a strong impact on the electrical conductivity of the substrate, which, in turn, regulates neural circuit outputs.



Carbon nanotubes (CNTs) have long been recognized for owning the perfect combination of strength and conductivity, both thermal and electrical, along with a large specific surface area characterized by low density.^{1,2} However, in general, CNTs are not suitable for practical applications, since they are produced in a powder and show poor processability for use at the macroscopic scale. In this sense, the research on CNT films (often called buckypapers) has blossomed during the past years,^{3–6} yielding materials with improved properties. Films of pure CNTs can be prepared by vacuum filtration methods;⁴ however, the mechanical performance and stability of *pristine* CNT films are still limited, as the interaction between adjacent CNTs takes place through weak π - π stacking and van der Waals forces.⁷ Chemical cross-linking of CNTs is a promising strategy for increasing the mechanical features and overcoming the aforementioned weaknesses of CNT films. A buckypaper made by covalently cross-linked CNTs would result in stronger interactions among CNTs, leading to higher tensile strength of the CNT films.^{6,8,9} In addition, networks of CNTs generated by cross-linking are expected to exhibit an interesting porous structure, beneficial for a wide number of applications.

Nowadays, chemical modification and assembly of CNTs into higher order constructs preserving CNTs founding

features is still a major challenge. The cross-linking process is obtained, in general, at the expense of a reduction in electrical conductivity, due, at least in part, to the disruption of the CNT structure *via* covalent bonding. Therefore, a compromise between the mechanical and electrical properties may be necessary, and the optimal cross-linking degree should be determined according to the desired final properties and applications.

Several methods have been proposed for cross-linking CNTs, including the use of long and flexible poly(ethylene glycol) chains,¹⁰ 1,4-benzoquinones,¹¹ aryl diazonium salts,¹² and polymer coating.¹³ More recently, Ku *et al.* demonstrated, through molecular dynamics and experimental studies, that the mechanical properties strongly depend on the degree of cross-linking, length of cross-linkers, and the diameter of the employed CNTs,¹⁴ and they proved that the incorporation of aromatic cross-linkers between carbon nanotube fibers enhances the mechanical properties without a significant loss of electrical conductivity. Hence, this method appears as a

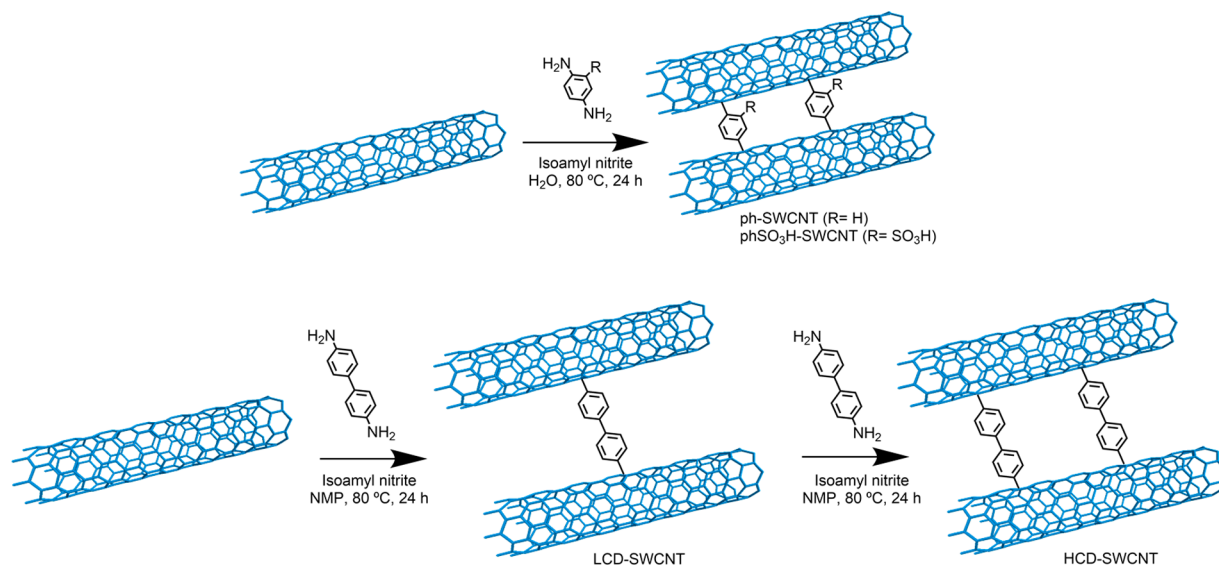


Figure 1. Diazonium salt cross-linking reaction routes to provide the interlinked SWCNTs.

promising methodology for the preparation of CNT films with interesting structural and electrical properties for a wide number of applications.

Among the potential applications of CNT films,¹⁵ an emerging field is that of neuroscience. CNT substrates promote cell viability and adhesion,¹⁶ and during the past decade many studies reported that CNTs enhance and guide axon growth and potentiate synapse formation and network activity^{16–22} as well as single neuron excitability, by providing a cell–substrate electrical coupling.¹⁷ When used to coat brain implants, CNTs are able to outperform traditional electrodes by enhancing recordings and stimulation from and to brain tissues, both *in vitro* and *in vivo*.^{23,24} Interestingly, CNT films contribute in reducing astrogliosis, affecting astrocyte morphology and proliferation,²¹ ultimately limiting glial scar formation.²²

To successfully promote neuronal growth, the CNT substrates should show high mechanical stability in order to provide a stable neural interface.¹⁶ High electrical conductivity is also crucial to achieve good stimulation of the neural cells.¹⁶ However, the development of CNT substrates with appropriate mechanical stability and good conductivity, applicable to the design of neuroimplantable devices, still remains a challenge. In this direction, the chemical modification of CNTs can be used to influence the CNT/neuronal interaction and modify cell behavior.²⁵ Most of the studies involving neural substrates that consist of covalently modified CNTs reported so far are based on oxidized materials.^{26–30} CNTs covalently functionalized with protein growth factors have also been described.³¹ Conducting polymers have also been used for the chemical modification of carbon nanotubes and their application for neuronal growth.^{32–34} However, this kind of hybrid material normally shows reduced electrical conductivity, a CNT feature shown to be relevant in neuronal interfacing.^{17,35,36} In other cases, patterned CNTs are used as scaffolds to support neurite outgrowth,³⁷ yielding fragile substrates that may lead to detachment of the CNTs during the implantation process, exposing potentially toxic scaffold materials.

In this framework, one of the major requirements to allow successful design of CNT-based devices in neurology is the development of conductive and freestanding structures with

high CNT content, covalently cross-linked materials with improved mechanical stability. Such freestanding CNT substrates could be simultaneously used to deliver controlled and precise electrical stimulus and to promote cell growth on a physical template of controlled porosity.

Herein we focus on the chemical cross-linking of single-walled carbon nanotubes (SWCNTs) through aromatic compounds, with the aim of achieving CNT substrates with upgraded mechanical properties, still maintaining interesting electroconductive behavior. We challenged the cross-linked SWCNT scaffolds, showing different conductive properties, with neuronal network growth and function.

RESULTS

Features of Manufactured CNT-Based Substrates.

SWCNTs were chosen for the formation of the cross-linked materials because of their high flexibility, a feature that could make the formation of the desired CNT meshes easier. Aryl diazonium salt chemistry, which has been widely used in the literature for grafting aryl groups to the surface of graphitic materials,^{38,39} was applied for the cross-linking of SWCNTs. For this purpose, *p*-phenylene diamino derivatives with different lengths were employed as cross-linkers, while the degree of entanglement was checked by varying the degree of functionalization. In detail, the cross-linking procedure was performed using *p*-phenylenediamine, 2,5-diaminobenzenesulfonic acid, and benzidine, yielding the products ph-SWCNT, phSO₃H-SWCNT, LCD-SWCNT, and HCD-SWCNT, respectively (Figure 1). LCD and HCD refer to the products resulting from the cross-linking with benzidine at low and high degrees of cross-linking, as reported in a previous work,⁴⁰ where the synthesis and characterization of LCD-SWCNT and HCD-SWCNT have been described.

The successful formation of the interlinked materials was followed by Raman spectroscopy, in combination with UV–Vis–NIR absorption spectroscopy, thermogravimetric analysis (TGA), atomic force microscopy (AFM), transmission electron microscopy (TEM), scanning electron microscopy (SEM), and conductivity measurements, to obtain fully detailed information about the structural, electronic, and chemical properties of the synthesized nanohybrids.

UV-vis-NIR absorption spectra were recorded for each material and compared with *pristine* SWCNTs (*p*-SWCNTs) (Figure S1). The spectrum corresponding to *p*-SWCNTs exhibits the typical van Hove singularities attributed to the different optical transitions. As expected, the cross-linking procedure resulted in the loss of the van Hove singularities. This loss of features is due to the alteration of the electronic structure, which is particularly indicative of sidewall functionalization.

Raman spectroscopy also provided efficient support to the successful cross-linking of SWCNTs (Figure S2 and Table 1).

Table 1. TGA, Raman and Conductivity Data for the Resulting Cross-Linked Materials

| material | TGA($\mu\text{mol/g}$) ^a | Raman I_D/I_G | σ (S/m) |
|---------------------------|---------------------------------------|-----------------|----------------|
| <i>p</i> -SWCNTs | | 0.06 | 3389 |
| Ph-SWCNT | 2023 | 0.27 | 56 |
| PhSO ₃ H-SWCNT | 1045 | 0.23 | 102 |
| LCD-SWCNT | 536 | 0.24 | 1083 |
| HCD-SWCNT | 944 | 0.39 | 81 |

^a μmol of functionalizing groups per gram of material.

The spectra performed using the 785 nm line laser show the typical peaks corresponding to the CNTs, that is, the radial breathing mode (RBM), between 180 and 280 cm^{-1} , and the two peaks corresponding to the disorder-induced D mode and the C-C stretching G mode, at 1295 and 1595 cm^{-1} , respectively. As observed, the intensity of the I_D/I_G ratio was higher for the cross-linked materials when compared to *p*-SWCNTs, as a consequence of the increase of the structural defects on the CNT sidewall after the cross-linking process. To get a deeper insight into the types of CNTs that were involved in the functionalization process (metallic or semiconducting), the RBM regions were analyzed. To this end, 532 and 633 nm laser lines were employed, since the 785 nm laser line is only in resonance with semiconducting CNTs. As shown in Figure S2d, where the RBM spectra are normalized to the mode of the nanotube with the largest diameter that was not affected by the functionalization (smallest Raman shift), the RBM intensities indicate that metallic CNTs are affected by the cross-linking process to a larger extent when compared to semiconducting CNTs. These results are in good agreement with previous studies that have revealed that the covalent functionalization of SWCNTs with diazonium salts takes place with high selectivity toward metallic CNTs.^{41,42}

The degree of functionalization was determined by TGA under nitrogen flow and consisted of heating ramps of 10 $^\circ\text{C}/\text{min}$ up to 800 $^\circ\text{C}$ (Figure S3 and Table 1). In order to facilitate the determination of the decomposition temperatures of the cross-linking agents, differential thermogravimetric (DTG) curves were superimposed (Figure S3).

From DTG curves, the initial decomposition temperatures of the weightlessness of the cross-linking agents were estimated as follows: around 280 $^\circ\text{C}$ for ph-SWCNT, 363 $^\circ\text{C}$ for phSO₃H-SWCNT, and 230 $^\circ\text{C}$ for LCD-SWCNTs and HCD-SWCNTs. These are completely removed at around 600, 580, and 380 $^\circ\text{C}$ for ph-SWCNT, phSO₃H-SWCNT, and LCD-/HCD-SWCNTs, respectively. The residual mass, once the cross-linking agents have been removed, is 68% for ph-SWCNT, 78% for phSO₃H-SWCNT, 91% for LCD-SWCNTs, and 86% for HCD-SWCNT, which might be attributed to the remaining mass of CNTs, probably corresponding to those

CNTs with larger diameters. TGA analysis allowed also the estimation of the functional group coverage (FGC) for each sample, which was estimated from the weight loss percentages (wt %) of the cross-linking agents (wt %_{linker}) and SWCNTs (wt %_{SWCNTs}) in each sample, and the molecular weights of the cross-linking agents (MW_{linker}) and atomic mass of carbon according to the following equation:⁴³

$$\text{FCG} = \frac{\text{wt \%}_{\text{SWCNTs}}/12.01}{\text{wt \%}_{\text{linker}}/MW_{\text{linker}}}$$

For this purpose, the wt % was determined from the mass loss in the TGA curves under N₂, at 600 $^\circ\text{C}$ for ph-SWCNT, at 550 $^\circ\text{C}$ for phSO₃H-SWCNT, and at 500 $^\circ\text{C}$ for LCD-SWCNTs and HCD-SWCNTs, where it is considered that the cross-linking agent has been completely removed from the CNT sidewall. According to this, the TGA curves developed a group coverage of 1 group every 23 carbon atoms (2023 $\mu\text{mol/g}$) and 1 group every 77 carbon atoms (1045 $\mu\text{mol/g}$) for Ph-SWCNT and PhSO₃H-SWCNT, respectively, in agreement with the results from the Raman studies presented above. For the longest linker consisting of two phenyl rings, the calculated group coverages were 1 group every 234 carbon atoms (536 $\mu\text{mol/g}$) and 1 group every 98 carbon atoms (944 $\mu\text{mol/g}$) for LCD-SWCNT and HCD-SWCNT, respectively, as previously described in the literature.⁴⁰ These latter results, along with the I_D/I_G values observed for both materials, confirmed the higher loading of linkers reached through the second round of functionalization.

Electrical conductivity studies were also performed for the synthesized materials and compared to those of *p*-SWCNTs. For this purpose, the van der Pauw method was employed.⁴⁴ Thin films were prepared using the vacuum filtration method, and the average membrane thickness was measured. The sheet resistance (R_s) was evaluated by means of a 4-point probe conductometer. For *p*-SWCNTs, Ph-SWCNT, and PhSO₃H-SWCNT, which did not show the free-standing structure required to be manipulated by tweezers, the conductivity was calculated without peeling off the materials from the surface of the PTFE filter. In order to avoid inaccurate readings due to the direct contact between the conductometer points and the filter, thick films of material were prepared. Electrical conductivity (σ) was then calculated from the measured R_s and the sample thickness (t), according to the formula $\sigma = 1/(R_s t)$. The data reported in Table 1 collect the results obtained from Raman, TGA, and conductivity measurements. As expected, *p*-SWCNTs presented the highest values of conductivity, which decreased after the disruption of the π - π structure by means of functionalization and, more so, with the increase of the functionalization degree, as clearly observed in the case of LCD-SWCNT relative to HCD-SWCNT. These results are consistent with the analysis previously performed on the RBM Raman regions (Figure S2d). The change toward less metallic behavior after the cross-linking process explains the decrease of conductivity observed for the cross-linked materials that is higher when the loading of cross-linking agent increases.

To better understand the topography and structure of the cross-linked materials, TEM and SEM studies were performed. TEM images revealed the existence of clear differences before and after the interlinking process. For Ph-SWCNT and PhSO₃H-SWCNT (Figure S4), larger meshes of nanotubes were observed after the functionalization process, indicating a successful covalent cross-linking of the CNTs. Considerable

differences were also observed by TEM between the LCD-SWCNT and HCD-SWCNT.⁴⁰ According to its paper-like physical appearance, the density of the meshwork was higher for LCD-SWCNTs in comparison with *p*-SWCNTs, and most notable, a dense meshwork of CNTs characterized by large surface roughness was observed for HCD-SWCNTs.⁴⁰ Similarly, a change in the surface morphology was observed by SEM between the *p*-SWCNTs and the interlinked materials. As observed, ph-SWCNT and phSO₃H-SWCNT (Figure S5) exhibited a more compacted rough surface when compared to the *pristine* material. In the case of LCD-SWCNT and HCD-SWCNT, the interlinked SWCNTs exhibited a network-like structure with a homogeneous distribution, leading to a large continuous wrinkled film of nanotubes.⁴⁰

To estimate the cross-linked SWCNTs' potential as substrates for neuronal growth, dissociated hippocampal cultures^{35,45} were seeded on LCD-SWCNTs and HCD-SWCNT. The choice of LCD-SWCNT and HCD-SWCNT for the study was motivated by the easy preparation of free-standing substrates in these cases, which is a prerequisite for their future application as substrates for neural growth in the injured tissue. It is important to note that Ph-SWCNT and PhSO₃H-SWCNT were obtained as powder samples after the functionalization process. Free-standing substrates were not achieved in these cases. Therefore, their manipulation in future implantation processes would not be a straightforward task. This, together with the fact that the electrical conductivity of Ph-SWCNT and PhSO₃H-SWCNT was very similar to that of HCD-SWCNT (see Table 1), led us to the decision of using only LCD-SWCNT and HCD-SWCNT for neural interfacing. On the other hand, the existence of considerably different values of electrical conductivity between LCD-SWCNT and HCD-SWCNT (1083 *vs* 81 S/m, respectively) allowed an interesting comparison about how this parameter affects neuronal behavior. These conductivity values are considerably better than those reported previously for MWCNTs chemically modified through the same approach,²⁵ which is probably attributable to the intrinsic conductivity of the *pristine* materials, which is much better in the case of the *p*-SWCNTs employed in the current work ($\sigma = 3389$ S/m for *p*-SWCNTs *vs* $\sigma = 625$ S/m for *p*-MWCNTs (calculated from the sheet resistance in ref 25)). After the functionalization process, higher loading of functional groups is achieved in the present work (944 $\mu\text{mol/g}$ for the SWCNTs with a higher degree of functionalization *vs* 230 $\mu\text{mol/g}$ for the MWCNTs with a higher degree of functionalization reported in ref 25). Even so, the electrical conductivity for the functionalized SWCNTs is around 200 times better than that reported for the highly functionalized MWCNTs ($\sigma = 0.341$ S/m and $\sigma = 81$ S/m for functionalized MWCNTs and SWCNTs, respectively), which suggest the promise of our cross-linked CNT-based substrates for the improvement of neuronal activity.

Confocal reconstructions and calcium imaging experiments were then performed to assess the behavior of the neural cells when seeded on the conductive CNT substrates.

Confocal Reconstructions of Hippocampal Cultures Interfaced to LCD-SWCNT and HCD-SWCNT Substrates.

To investigate neuronal network formation and growth when integrated with the SWCNT films, we used rat dissociated hippocampal cultures.^{17,35,36} Cultured biosystems allow reliable *in vitro* reconstruction of synaptic connections among heterogeneous neuronal phenotypes in the presence of neuroglial cells and are brain-circuit models instrumental to

investigate *ad hoc* manufactured materials for interfacing neuronal activity.

Primary neurons from rat hippocampus were plated on LCD- and HCD-SWCNT films and, as control condition, on poly-L-ornithine-treated glass slides. Cells were cultured into functional synaptic networks. Cell morphology and adhesion to SWCNT substrates were assessed by immunofluorescence labeling and confocal microscopy. Figure 2A shows representative TEM images of the two different substrates. We compared neurons grown on poly-L-ornithine (control) substrates with those grown on SWCNT scaffolds, after 9–11 days *in vitro* (DIV). To prove the compatibility of both LCD- and HCD-SWCNT substrates, we imaged by immuno-

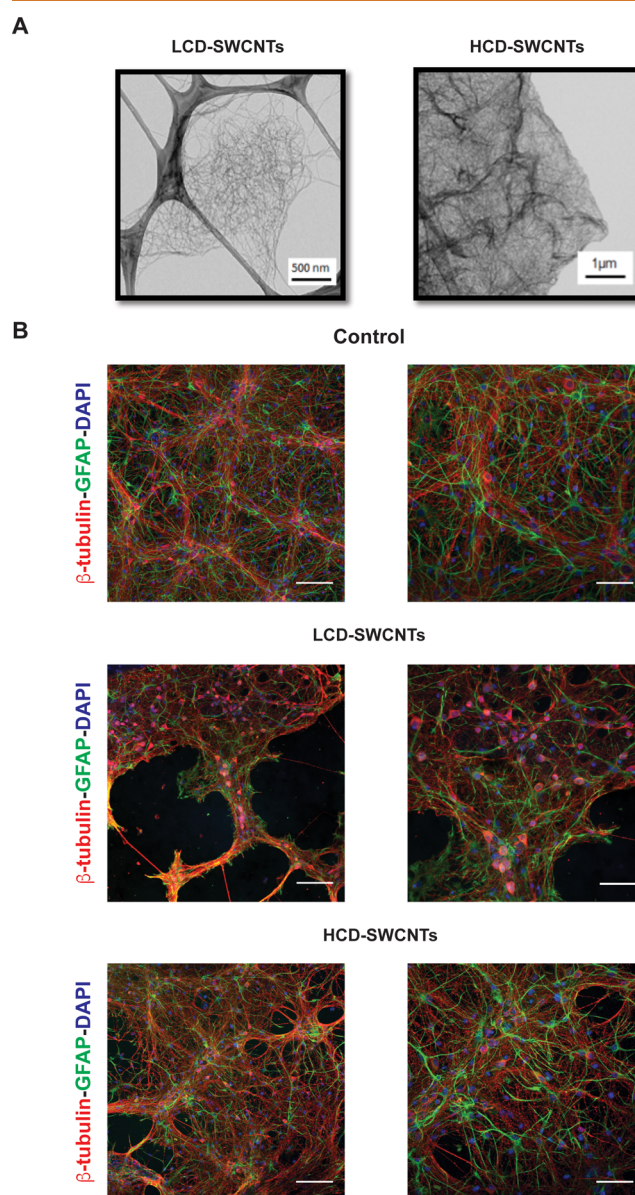


Figure 2. (A) TEM images for LCD-SWCNT (left) and HCD-SWCNT (right) substrates. (B) Confocal micrographs showing hippocampal cultures grown (10 DIV) on control (top), LCD-SWCNT (middle), and HCD-SWCNT (bottom) substrates immune-stained for β -tubulin III (in red), GFAP (in green), and DAPI (blue) at lower (left panel) and higher magnification (right panel). Scale bar: 100 μm (left) and 50 μm (right).

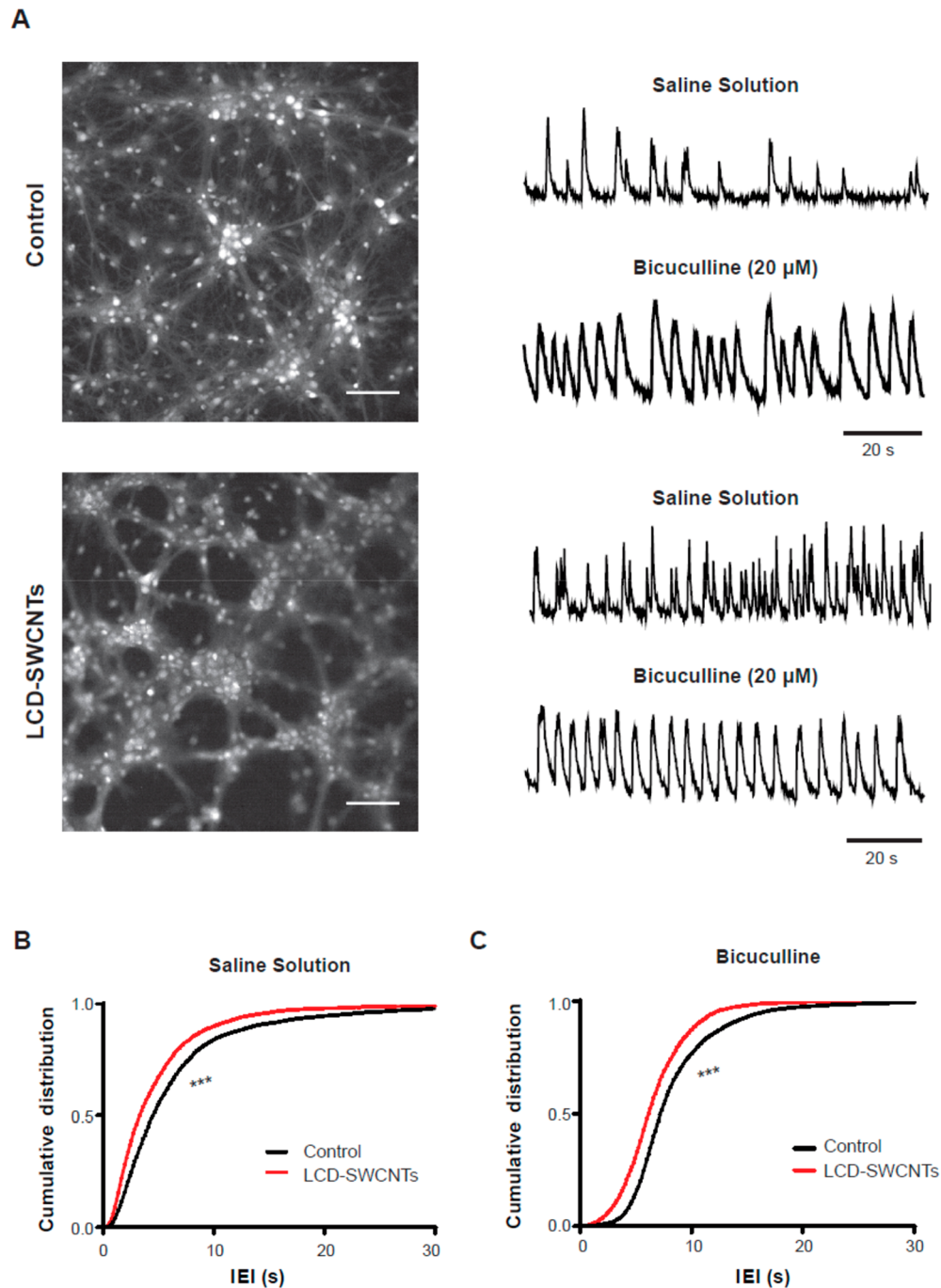


Figure 3. (A) (left) Snapshots of representative fields of neuronal cultures grown on control (top) and LCD-SWCNT (bottom) substrates, stained with Oregon Green 488-BAPTA-1 AM. Scale bar: 50 μm . (A) (right) Repetitive Ca^{2+} events spontaneously (top) or bicuculline-induced (bottom) recorded in hippocampal cultures of 10 DIV. (B) Cumulative distribution of IEI values recorded in saline solution of control (black) and LCD (red) cells (***) $p < 0.0001$; Kolmogorov–Smirnov test). (C) Cumulative distribution of bicuculline-induced IEI values of control (black) and LCD (red) cells (***) $p < 0.0001$; Kolmogorov–Smirnov test).

fluorescence the specific cytoskeletal components β -tubulin III, to identify neurons and glial fibrillary acidic protein (GFAP) for astrocytes.^{36,46,47} In all cultures tested ($n = 33$ visual fields for the three different conditions), before fixation for confocal microscopy, live neuronal calcium activity was monitored.

Figure 2B shows low (left panels) and high (right panels) magnification confocal micrographs with β -tubulin III-positive cells (in red) and GFAP-positive ones (in green) developed in control (top) or in the synthesized LCD-SWCNT (middle) and HCD-SWCNT (bottom) substrates; in all images nuclei

are visualized by DAPI (in blue). TEM images for LCD- and HCD-SWCNTs are shown in A to provide further insight into the morphology of each substrate.

Both neurons and neuroglia cells matured once on SWCNT supports, as shown in Figure 2B (high magnification) by the outgrowth of axons and dendrites in the case of neurons^{36,46} and by the stellate shape of GFAP+ cells,^{36,48} leading to the development of a complex network covering the entire SWCNT surface. We further compared cell densities among LCD-SWCNTs, HCD-SWCNTs, and control cultures. LCD-

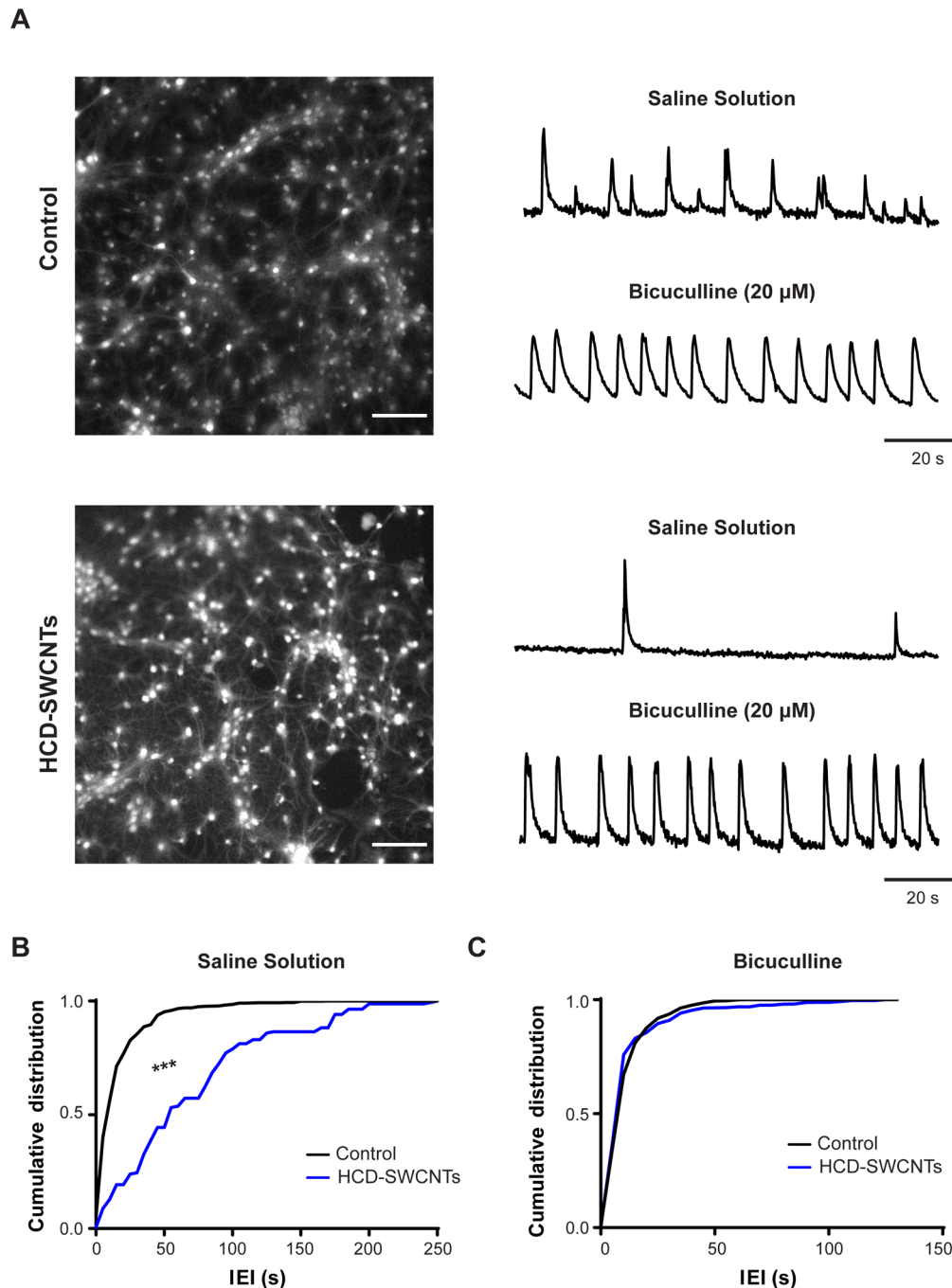


Figure 4. (A) (left) Snapshots of representative fields of neuronal cultures grown on control (top) and HCD-SWCNT (bottom) substrates, stained with Oregon Green 488-BAPTA-1 AM. Scale bar: 50 μm . (A) (right) Repetitive Ca^{2+} events spontaneously (top) or bicuculline-induced (bottom) recorded in hippocampal cultures of 10 DIV. (B) Cumulative distribution of IEI values recorded in saline solution of control (black) and HCD (blue) cells ($***p < 0.0001$; Kolmogorov–Smirnov test). (C) Cumulative distribution of bicuculline-induced IEI values of control (black) and HCD (blue) cells ($***p < 0.0001$; Kolmogorov–Smirnov test).

and HCD-SWCNTs and controls supported neuron and neuroglia growth in a similar manner, as highlighted by cell density measures (for neurons, in controls, 140 ± 35 β -tubulin-positive cells/ mm^2 ; in LCD-SWCNTs, 110 ± 29 β -tubulin-positive cells/ mm^2 ; in HCD-SWCNTs, 138 ± 35 β -tubulin-positive cells/ mm^2 ; for neuroglia, in controls, 110 ± 20 GFAP-positive cells/ mm^2 ; in LCD-SWCNTs, 120 ± 25 GFAP-positive cells/ mm^2 ; in HCD-SWCNTs, 118 ± 20 GFAP-positive cells/ mm^2 ; $n = 11$ visual fields per condition, three independent culture series). Thus, both LCD- and HCD-

SWCNT membranes allowed attachment and growth of rat hippocampal neurons displaying mature morphology.

Live Imaging of Hippocampal Cultures Interfaced to LCD-SWCNT and HCD-SWCNT Substrates. To study the emergence of neuronal activity by the networks formed interfaced to LCD-SWCNT and HCD-SWCNT substrates, we used fluorescent calcium imaging.^{49,50} After 8–10 DIV, neurons mature and generate synaptic signaling spontaneously, involving the activation of glutamate and GABA_A receptor-mediated synapses,^{45,51} the major central nervous system

(CNS) neurotransmitters for fast synaptic communication. We compared activity emerging from neurons, cultured on control and LCD- and HCD-SWCNT substrates (Figures 3 and 4). Neurons loaded with the membrane-permeable Ca^{2+} dye Oregon Green 488 BAPTA-1 were simultaneously visualized within the sampled area, and on average 20 ± 4 fluorescent cells were analyzed in each visual field ($680 \times 680 \mu\text{m}^2$; Figures 3A and 4A, left panels).

The experiments were performed at 9–11 DIV when neurons, intensely connected by synapses, display spontaneous activity in the form of bursts of activity, emerging by irregular synchronized firing events,^{17,36,52} generating transient episodes of calcium rise from the baseline (Figures 3 and 4).^{36,52–54} In the control, spontaneous Ca^{2+} activity was detected in 67% of the recorded neurons (172 out of 257 neurons), visualized in each field ($n = 10$ fields). Notably, in LCD-SWCNTs virtually all (>98%, 133 out of 136 neurons; $n = 6$ fields) were active and generated spontaneous, repetitive Ca^{2+} episodes. Figure 3A (right) shows examples of fluorescent recordings of active cells sampled from control and LCD-SWCNT substrates. Spontaneous episodes of activity appear as bursts of synaptic, action potential dependent events and are blocked by application of tetrodotoxin (TTX, $1 \mu\text{M}$; a toxin that targets voltage-dependent sodium channels). We measured the amount of Ca^{2+} episodes occurring in spontaneously active cells, and we quantified the interevent interval (IEI), the interval of time between the onset of a calcium wave and the beginning of the next one, which is significantly ($***p < 0.0001$; Kolmogorov–Smirnov test) shorter in LCD-SWCNT substrates (on average 8 ± 4 s, $n = 133$ cells, from 3 different series of cultures) when compared to control ones (14 ± 4 s, $n = 172$ cells, from 3 different series of cultures; see the IEI cumulative distribution in Figure 3B), strongly indicative of a different functional organization due to the presence of LCD-SWCNTs.

In a second group of experiments we blocked inhibitory synaptic transmission by bicuculline ($20 \mu\text{M}$) application. This antagonist of GABA_A receptors is known to alter the profile of network activity^{55,56} from random bursting to synchrony, characterized by more intense and regular bursting.^{53,54} As shown in Figure 3A, active cells upon bicuculline exposure generate Ca^{2+} events with an IEI of, on average, 4 ± 0.9 s in LCD-SWCNT neurons ($n = 133$), a value significantly ($p < 0.001$) lower when compared to that of the control (on average 8 ± 3 s; $n = 172$ cells; see the cumulative distribution plot in Figure 3C). Such disinhibited episodes were completely abolished by TTX applications, confirming their neuronal origin. Figure 4A (right panel) shows representative fluorescent tracings from active cells recorded in HCD-SWCNTs; notably Ca^{2+} spontaneous activity was detected only in 21% (34 out of 162 neurons; HCD-SWCNTs) of the cells visualized in each field ($n = 6$ fields), a very low value when compared to their relative control (65%; 97 out of 149 neurons; $n = 6$ fields). When we measured the spontaneous Ca^{2+} activity, the IEI was significantly ($***p < 0.0001$; Kolmogorov–Smirnov test) longer in HCD-SWCNT substrates (on average 72 ± 10 s, $n = 34$ cells, from 3 different series of cultures) when compared to control ones (on average 17 ± 7 s, $n = 97$ cells, from 3 different series of cultures; see also cumulative distribution in Figure 4B). However, upon pharmacological removal of synaptic inhibition (Figure 4C), an IEI similar to the control was restored (HCD-SWCNT substrates on average 8 ± 5 s, $n = 34$ cells; control substrates

on average 10 ± 3 s, $n = 97$ cells). Thus, apparently, the different substrates promote the formation of diverse networks; in particular the inhibitory control on HCD-SWCNTs appeared to be strongly developed in these cultured brain circuits when compared to LCD-SWCNTs and the control, while LCD-SWCNTs, as expected, boosted network activity in all network states (resting and disinhibited).

DISCUSSION

The present study provides important insight into how the electrical conductivity of the CNT free-standing substrates affects the growth and electrical properties of cultured hippocampal networks. The cross-linking of SWCNTs with diamino-phenyl derivatives has provided an efficient route to design free-standing CNT substrates with tunable electrical properties, which is promising for applications in neural tissue engineering. Raman and electrical studies demonstrated that the electrical conductivity of the final materials is directly related to the type of cross-linker and the degree of functionalization (Table 1). In the particular case of benzidine as cross-linker, an important decrease of the electrical conductivity was observed when increasing the degree of functionalization by 40% (1083 S/m for LCD-SWCNT vs 81 S/m for HCD-SWCNT), allowing the preparation of free-standing neuronal substrates with different electrical properties. Both LCD-SWCNTs and HCD-SWCNTs have been employed as substrates for interfacing neural cells. The most important finding of the study is that neuronal circuits chronically interfaced to SWCNT substrates can be effectively affected by the CNTs' degree of functionalization. Cultured brain circuits represent the simplest *in vitro* model of brain network. The morphology and cell phenotype distribution of hippocampal networks did not differ when developed on control glass surfaces or on LCD- and HCD-SWCNT carpets. The two cellular networks are made of healthy and functional cells, indicating the cytocompatibility of both SWCNT substrates (Figure 2B).³⁵

Conversely, when investigating network dynamics by monitoring intracellular calcium activity, we observed significant differences comparing LCD-SWCNT substrates with HCD ones. Live calcium episodes, whose neuronal and synaptic nature was supported by TTX experiments,⁵⁴ reflected the spontaneous activation of synapses, typical of these preparations.¹⁷ Specifically, such synchronized synaptic activations are an accepted measure of neural network dynamics.⁵³

We speculated that LCD-SWCNT substrates within their range of conductivity and functionalization could enhance neuronal activity (Figure 3), in a way similar to what happens with MWCNTs.^{17,25,35,57} In fact, in interfacing hippocampal neurons with LCD-SWCNT substrates, we reproduced CNTs' ability to support signaling and synchronization in cultured circuits.^{17,45} Our results confirmed that neuronal physiological and synaptic efficacy could be tuned by specific neuron–surface interactions, in particular when using electrically conductive growth interfaces.^{25,35,36,58}

We, in fact, observed that neurons grown on LCD-SWCNTs generate bursts with higher rate, with or without inhibition, potentially due to an improved efficiency in axonal signaling and to the increase in synaptic connections^{17,35,36,58} (Figure 3). We favor the hypothesis that the LCD-SWCNTs' ability to alter cellular excitability could significantly contribute to the

described results. In fact, the higher the cellular excitability, the higher would be the probability of finding active cells.^{36,59,60}

As the degree of functionalization increases, this effect on the emerging neuronal activity decreased (Figure 4). This effect is not attributable to differences in neuronal survival or morphology (Figure 3), but possibly represents a consequence of the properties of the SWCNT substrates and could primarily result from specific synaptic interactions.⁶¹

In fact, reducing the conductivity of the substrates, we observed a significant decrease in terms of active cells and the emerging spontaneous activity. We cannot exclude that HCD-SWCNTs interfere with the maturation of inhibitory neurons and the network composition. In this hypothesis, HCD-SWCNTs may favor more mature chloride ion fluxes through GABA_A receptors. In neurons, the amplitude of the inhibitory currents is governed by the intracellular chloride concentration and, in more mature stages of development, goes from higher to lower values, with respect to the extracellular milieu.⁶² Thus, in HCD-SWCNTs, there could be a higher fraction of effective inhibitory neurons, thus biasing the spontaneous network activity.

On the basis of our results, we may propose that HCD-SWCNT properties are responsible for a different maturation in cellular organization. However, even under these conditions, the block of GABA_A receptor-mediated inhibition boosted Ca²⁺ episodes as in control conditions, suggesting a similar role of inhibition in counteracting excitability in the synaptic network.

Hu and collaborators³⁰ found that the chemical functionalization of CNTs with different molecules is able to control the outgrowth and branching of neuronal processes. Accordingly, Malarkey and co-workers reported that SWCNT scaffolds with different conductivities affected rat hippocampal neuron neurite outgrowth.²⁷ Our current results are also in agreement with our recent report²⁵ where the impact of MWCNT growth substrates on cell development and signaling depended on their degree of functionalization and on the functionalized groups. In that work,²⁵ despite the absence of changes in network size in all the functionalization conditions tested, we measured an increased synaptic activity only in those neurons interfaced to the MWCNTs with the lowest functionalization degree.

Although we cannot exclude such modulations, the simple tuning of neurite outgrowth would not explain the similar activity obtained in bicuculline when applied in control and HCD-SWCNTs; thus we favor the hypothesis that the conductivity of CNTs might regulate network excitability and synapse formation.^{17,35}

Overall, our results demonstrate that SWCNTs can be systematically manipulated and functionalized to display different electrical properties.

These results show that SWCNT structuring *via* cross-linking is a key factor to successfully use CNT-based substrates for biomedical applications or tissue engineering. For their peculiar chemical and electrical properties, as well as their functionalization degree, LCD-SWCNTs seem to be the most promising cross-linked substrate for the design of neuronal interfaces of the future.

Characterizing the interactions between CNTs and brain cells and their circuitry together with how the quality of conductivity affects their functionality offer developments for applying nanotechnology to and for the nervous system.

CONCLUSIONS

In this work, a facile and promising method based on chemical cross-linking of carbon nanotubes is employed for controlling the electrical conductivity of CNT-based substrates. We have developed a method to simultaneously obtain free-standing CNT-based substrates and tune the electrical properties of the final materials. Immunofluorescence studies and calcium imaging demonstrated that neural activity can be regulated by modifying the electrical properties of the CNT-based substrates, while maintaining neuronal growth unaffected. These findings may provide possibilities for controlling the electrical properties of future implantable neuronal interfaces.

EXPERIMENTAL SECTION

Materials. All the chemicals and solvents were purchased from Sigma-Aldrich and used without any further purification. Single-walled carbon nanotubes HiPco were purchased from Nanointegris (purified grade, length = 100–1000 nm, diameter ~0.8–1.2 nm, <15% remaining iron particles) and used without further purification treatment.

Synthesis: General Procedure for the Synthesis of Cross-Linked SWCNTs. A 100 mg amount of *p*-SWCNTs was dispersed in 150 mL of *N*-methyl-2-pyrrolidone (NMP) and sonicated for 15 min. A 100 mg amount of the corresponding phenyl derivative and 0.5 mL of isopentyl nitrite were added, and the reaction mixture was stirred for 24 h at 80 °C. The crude was filtered through a PTFE membrane with an average pore size of 0.45 μm, and the black precipitate was washed several times with NMP, methanol, and diethyl ether. The resulting material was dried under vacuum and weighed.

Characterization Methods. UV–vis–NIR measurements were carried out on a Cary 5000 spectrometer (Varian), using 1 cm path quartz cuvettes. Thermogravimetric analyses were performed using a TGA Q500 (TA Instruments). Raman spectra were obtained on a Renishaw inVia Raman microscope at room temperature with an exciting laser source ($\lambda = 785 \text{ cm}^{-1}$). Measurements were taken with 10 s of exposure time, and the laser spot was focused on the sample surface using a long working distance 50× objective. Raman spectra were collected on numerous spots on the sample and recorded with a Philips SPC1030NC camera. AFM images were acquired in tapping mode using a Multimode V7.30 (Veeco Instruments Inc., Santa Barbara, CA, USA) with a NanoScope V controller (Digital Instruments, Santa Barbara, CA, USA). The cantilevers (HQ:NSC15/Al BS probes from Mikromasch) were silicon cantilevers with a resonance frequency of 325 kHz and a nominal force constant of 40 N m⁻¹. The images were processed using WSxM (freely downloadable scanning probe microscopy software (www.nanotec.es)). TEM images were recorded on a Philips EM208 TEM using iTEM software (Olympus Soft Imaging Solutions GmbH, Münster, Germany). About 1 mg of material was dispersed in 5 mL of EtOH and sonicated for 30 min. Then one drop of this solution was deposited on a TEM grid (lacey carbon film, copper, 300 mesh). SEM images were acquired by collecting secondary electrons on a commercial SEM (Gemini SUPRA 40, Carl Zeiss NTS GmbH, Oberkochen, Germany). For the analysis, the different materials were placed on conductive double-sided carbon tape (Ted Pella, Inc., USA) and imaged at 5 keV. For the powdered samples (ph-SWCNT and phSO₃H-SWCNT), about 1 mg of material was placed on the double-sided carbon tape previously attached to the SEM stub and was pressed lightly to adhere the sample to the tape. In the case of LCD- and HCD-SWCNTs a piece of material was sectioned using a scalpel and mounted on the SEM stub using the double-sided carbon tape. Resistance was collected using a Jandel four-point probe analyzer (RM-3000), and conductivity was calculated applying Ohm's law. For this purpose, the required films were prepared through filtration of 1 mg of material on a PTFE filter (Millipore 0.45 μm pores), and the membrane thickness was measured with a micrometer (High-Accuracy Digimatic micrometer 293-100, Mitutoyo).

Preparation of Primary Hippocampal Cultures. Primary dissociated cultures were prepared from postnatal (P2–P3) rats as previously reported.^{17,30,42} All procedures were approved by the local veterinary authorities and performed in accordance with the Italian law (decree 116/92) and the EU guidelines (86/609/CE, 2007/526/CE, and 2010/63/UE). Animal use was approved by the Italian Ministry of Health. All efforts were made to minimize animal suffering and to reduce the number of animals used. Cells were plated on poly-L-ornithine-coated glass coverslips and on HCD-SWCNT and LCD-SWCNT carpets. Before using for culturing, both SWCNT substrates were mounted on the glass coverslips (12 × 24 mm², 0.13–0.16 mm thick, Kindler, EU) by a thin adhesive layer of PDMS cured at 120 °C. One hour prior to plating, CNT substrates were treated with an air-plasma cleaner in order to facilitate cell adhesion^{36,63} and at the end sterilized with a UV lamp.

Calcium Imaging. Cultures were loaded with the cell-permeable Ca²⁺ dye Oregon Green 488 BAPTA-1 AM (Invitrogen). A 4 mM stock solution of the Ca²⁺ dye was prepared in DMSO, and cultures were incubated with a final concentration of 4 μM for 40 min (37 °C; 5% CO₂).^{30,42} The samples were then placed in a recording chamber mounted on an inverted microscope (Nikon Eclipse Ti-U), where they were continuously superfused at room temperature (RT) by recording a solution of the following composition (mM): 150 NaCl, 4 KCl, 1 MgCl₂, 2 CaCl₂, 10 HEPES, 10 glucose (pH adjusted to 7.4 with NaOH), to continuously supply nutrients to the tissue. Cultures were observed with a 20× objective (0.45 NA), and recordings were performed from visual fields (680 × 680 μm², binning 4). Ca²⁺ dye was excited at 488 nm with a mercury lamp; excitation light was separated from the light emitted from the sample using a 395 nm dichroic mirror and ND filter (1/32). Images were continuously acquired (exposure time 150 ms) using an ORCA-Flash4.0 V2 sCMOS camera (Hamamatsu). The imaging system was controlled by integrating imaging software (HCImage Live). In order to induce a rhythmic burst, 20 μM bicuculline methiodide was bath-applied after a 10 min recording. At the end of each experiment, TTX (1 μM, a voltage-gated, fast Na⁺ channel blocker; Latoxan) was applied to confirm the neuronal nature of the recorded signals. Recorded images were analyzed off-line both with Fiji (selecting a region of interest, ROI, around cell bodies) and Clampfit software (pClamp suite, 10.2 version; Molecular Devices LLC, USA). Intracellular Ca²⁺ transients were expressed as fractional amplitude increase ($\Delta F/F_0$, where F_0 is the baseline fluorescence level and ΔF is the rise over baseline); we determine the onset time of neuronal activation by detecting those events in the fluorescence signal that exceed at least 5 times the standard deviation of the noise.

Immunocytochemistry and Image Processing. After 9–11 days *in vitro* hippocampal neurons and glial cells were fixed by 4% formaldehyde (prepared from fresh paraformaldehyde; Sigma) in phosphate-buffered saline (PBS) for 20 min, at RT. After that, cells were washed three times with PBS and permeabilized with 1% Triton X-100 for 30 min, blocked with 5% fetal bovine serum in PBS for 30 min at room temperature, and incubated with primary antibodies for 45 min. The primary antibodies used were as follows: rabbit polyclonal anti-β-tubulin III (1:500 dilution) and mouse monoclonal anti-GFAP (1:500 dilution). After PBS washes, cells were incubated for 45 min with AlexaFluor 594 goat anti-rabbit (Invitrogen, dilution 1:500) and AlexaFluor 488 goat anti-mouse (Invitrogen, dilution 1:500). Samples were mounted in Vectashield with DAPI in order to stain the nuclei (Vector Laboratories) on 1 mm thick coverslips. Images were acquired using a Nikon C2 confocal microscope (Nikon, Japan) at 40× magnification. Z-stacks were acquired every 500 nm, from seven to 10 random fields for control and SWCNT substrates. Offline analysis was performed using the image-processing package Fiji.

ASSOCIATED CONTENT

Supporting Information

The Supporting Information is available free of charge on the ACS Publications website at DOI: 10.1021/acsnano.9b02429.

Figures of UV–vis plots of the cross-linked materials in comparison with *p*-SWCNTs; Raman plots of the cross-linked materials in comparison with *p*-SWCNTs; TGA plots of the cross-linked materials in comparison with *p*-SWCNTs; TEM images of *p*-SWCNTs, ph-SWCNTs, and phSO₃H-SWCNTs; SEM images of *p*-SWCNTs, ph-SWCNTs, and phSO₃H-SWCNTs (PDF)

AUTHOR INFORMATION

Corresponding Authors

*E-mail: prato@units.it (M.P.).

*E-mail: ballerin@sissa.it (L.B.).

ORCID

Myriam Barrejón: 0000-0001-7218-066X

Laura Ballerini: 0000-0001-8420-0787

Maurizio Prato: 0000-0002-8869-8612

Author Contributions

[†]M.B. and R.R. contributed equally to this work.

Notes

The authors declare no competing financial interest.

ACKNOWLEDGMENTS

This work was supported by the Spanish Ministry of Economy and Competitiveness MINECO (project CTQ2016-76721-R), by the University of Trieste, Consorzio Interuniversitario Nazionale per la Scienza e Tecnologia dei Materiali (INSTM), Ministero dell'Università e della Ricerca (MIUR) (FIRB Prot. RBAP11ETKA and Cofin. Prot. 2010N3T9M4), and by the ByAxon no. 737116. M.P., as the recipient of the AXA Chair, is grateful to the AXA Research Fund for financial support. This work was performed under the Maria de Maeztu Units of Excellence Program from the Spanish State Research Agency, Grant No. MDM-2017-0720

REFERENCES

- (1) Hirsch, A. The Era of Carbon Allotropes. *Nat. Mater.* **2010**, *9*, 868–871.
- (2) Tasis, D.; Tagmatarchis, N.; Bianco, A.; Prato, M. Chemistry of Carbon Nanotubes. *Chem. Rev.* **2006**, *106*, 1105–1136.
- (3) Sreekumar, T. V.; Liu, T.; Kumar, S.; Ericson, L. M.; Hauge, R. H.; Smalley, R. E. Single-Wall Carbon Nanotube Films. *Chem. Mater.* **2003**, *15*, 175–178.
- (4) Gu, B. H.; Swager, T. M. Fabrication of Free-Standing, Conductive, and Transparent Carbon Nanotube Films. *Adv. Mater.* **2008**, *20*, 4433–4437.
- (5) Zhang, L.; Zhang, G.; Liu, C.; Fan, S. High-Density Carbon Nanotube Buckypapers with Superior Transport and Mechanical Properties. *Nano Lett.* **2012**, *12*, 4848–4852.
- (6) Jakubinek, M. B.; Ashrafi, B.; Guan, J.; Johnson, M. B.; White, M. A.; Simard, B. 3D Chemically Cross-Linked Single-Walled Carbon Nanotube Buckypapers. *RSC Adv.* **2014**, *4*, 57564–57573.
- (7) Behabtu, N.; Green, M. J.; Pasquali, M. Carbon Nanotube-Based Neat Fibers. *Nano Today* **2008**, *3*, 24–34.
- (8) Yu, Q.; Alvarez, N. T.; Miller, P.; Malik, R.; Haase, M. R.; Schulz, M.; Shanov, V.; Zhu, X. Mechanical Strength Improvements of Carbon Nanotube Threads through Epoxy Cross-Linking. *Materials* **2016**, *9*, 1–12.
- (9) Schirowski, M.; Abellán, G.; Nuin, E.; Pampel, J.; Dolle, C.; Wedler, V.; Fellingner, T. P.; Spiecker, E.; Hauke, F.; Hirsch, A. Fundamental Insights into the Reductive Covalent Cross-Linking of Single-Walled Carbon Nanotubes. *J. Am. Chem. Soc.* **2018**, *140*, 3352–3360.

- (10) Holzinger, M.; Steinmetz, J.; Samaille, D.; Glerup, M.; Paillet, M.; Bernier, P.; Ley, L.; Graupner, R. [2 + 1] Cycloaddition for Cross-Linking SWCNTs. *Carbon* **2004**, *42*, 941–947.
- (11) Ventura, D. N.; Stone, R. A.; Chen, K. S.; Hariri, H. H.; Riddle, K. A.; Fellers, T. J.; Yun, C. S.; Strouse, G. F.; Kroto, H. W.; Acquah, S. F. A. Assembly of Cross-Linked Multi-Walled Carbon Nanotube Mats. *Carbon* **2010**, *48*, 987–994.
- (12) Kumar, R.; Rao, C. N. R. Assemblies of Single-Walled Carbon Nanotubes Generated by Covalent Cross-Linking with Organic Linkers. *J. Mater. Chem. A* **2015**, *3*, 6747–6750.
- (13) Zhang, Y.; Broekhuis, A. A.; Stuart, M. C. A.; Fernandez, T.; Fausti, D.; Rudolf, P.; Picchioni, F. Cross-Linking of Multiwalled Carbon Nanotubes with Polymeric Amines. *Macromolecules* **2008**, *41*, 6141–6146.
- (14) Park, O. K.; Choi, H.; Jeong, H.; Jung, Y.; Yu, J.; Lee, J. K.; Hwang, J. Y.; Kim, S. M.; Jeong, Y.; Park, C. R.; Endo, M.; Ku, B. C. High-Modulus and Strength Carbon Nanotube Fibers Using Molecular Cross-Linking. *Carbon* **2017**, *118*, 413–421.
- (15) Hu, L.; Hecht, D. S.; Gru, G. Carbon Nanotube Thin Films : Fabrication, Properties, and Applications. *Chem. Rev.* **2010**, *110*, 5790–5844.
- (16) Marchesan, S.; Ballerini, L.; Maurizio, P. Nanomaterials for Stimulating Nerve Growth. *Science* **2017**, *356*, 1010–1012.
- (17) Cellot, G.; Cilia, E.; Cipollone, S.; Rancic, V.; Sucapane, A.; Giordani, S.; Gambazzi, L.; Markram, H.; Grandolfo, M.; Scaini, D.; Gelain, F.; Casalis, L.; Prato, M.; Giugliano, M.; Ballerini, L. Carbon Nanotubes Might Improve Neuronal Performance by Favouring Electrical Shortcuts. *Nat. Nanotechnol.* **2009**, *4*, 126–133.
- (18) Bosi, S.; Fabbro, A.; Ballerini, L.; Prato, M. Carbon Nanotubes: A Promise for Nerve Tissue Engineering. *Nanotechnol. Rev.* **2013**, *2*, 47–57.
- (19) Sucapane, A.; Cellot, G.; Prato, M.; Giugliano, M.; Parpura, V.; Ballerini, L. Interactions Between Cultured Neurons and Carbon Nanotubes: A Nanoneuroscience Vignette. *J. Nanoneurosci.* **2009**, *1*, 10–16.
- (20) Fan, L.; Feng, C.; Zhao, W.; Qian, L.; Wang, Y.; Li, Y. Directional Neurite Outgrowth on Superaligned Carbon Nanotube Yarn Patterned Substrate. *Nano Lett.* **2012**, *12*, 3668–3673.
- (21) Gottipati, M. K.; Samuelson, J. J.; Kalinina, I.; Bekyarova, E.; Haddon, R. C.; Parpura, V. Chemically Functionalized Single-Walled Carbon Nanotube Films Modulate the Morpho-Functional and Proliferative Characteristics of Astrocytes. *Nano Lett.* **2013**, *13*, 4387–4392.
- (22) Usmani, S.; Aurand, E. R.; Medelin, M.; Fabbro, A.; Scaini, D.; Laishram, J.; Rosselli, F. B.; Ansuini, A.; Zoccolan, D.; Scarselli, M.; Crescenzi, M. De; Bosi, S.; Prato, M.; Ballerini, L. 3D Meshes of Carbon Nanotubes Guide Functional Reconnection of Segregated Spinal Explants. *Sci. Adv.* **2016**, *2*, No. e1600087.
- (23) Keefer, E. W.; Botterman, B. R.; Romero, M. I.; Rossi, A. F.; Gross, G. W. Carbon Nanotube Coating Improves Neuronal Recordings. *Nat. Nanotechnol.* **2008**, *3*, 1–6.
- (24) Ansaldo, A.; Castagnola, E.; Maggolini, E.; Fadiga, L.; Ricci, D. Superior Electrochemical Performance of Carbon Nanotubes Directly Grown on Sharp Microelectrodes. *ACS Nano* **2011**, *5*, 2206–2214.
- (25) Bosi, S.; Fabbro, A.; Cantarutti, C.; Mihajlovic, M.; Ballerini, L.; Prato, M. Carbon Based Substrates for Interfacing Neurons: Comparing Pristine with Functionalized Carbon Nanotubes Effects on Cultured Neuronal Networks. *Carbon* **2016**, *97*, 87–91.
- (26) Hu, H.; Ni, Y.; Mandal, S. K.; Montana, V.; Zhao, B.; Haddon, R. C.; Parpura, V. Polyethyleneimine Functionalized Single-Walled Carbon Nanotubes as a Substrate for Neuronal Growth. *J. Phys. Chem. B* **2005**, *109*, 4285–4289.
- (27) Malarkey, E. B.; Fisher, K. A.; Bekyarova, E.; Liu, W.; Haddon, R. C.; Parpura, V. Conductive Single-Walled Carbon Nanotube Substrates Modulate Neuronal Growth. *Nano Lett.* **2009**, *9*, 264–268.
- (28) Liu, J.; Appaix, F.; Bibari, O.; Marchand, G.; Benabid, A. L.; Sauter-Starace, F.; Waard, M. De. Control of Neuronal Network Organization by Chemical Surface Functionalization of Multi-Walled Carbon Nanotube Arrays. *Nanotechnology* **2011**, *22*, 19S101.
- (29) Lee, H. J.; Yoon, O. J.; Kim, D. H.; Jang, Y. M.; Kim, H. W.; Lee, W. B.; Lee, N. E.; Kim, S. S. Neurite Outgrowth on Nanocomposite Scaffolds Synthesized from PLGA and Carboxylated Carbon Nanotubes. *Adv. Eng. Mater.* **2009**, *11*, B261–B266.
- (30) Hu, H.; Ni, Y.; Montana, V.; Haddon, R. C.; Parpura, V. Chemically Functionalized Carbon Nanotubes as Substrates for Neuronal Growth. *Nano Lett.* **2004**, *4*, 14–16.
- (31) Matsumoto, K.; Sato, C.; Naka, Y.; Kitazawa, A.; Whitby, R. L. D.; Shimizu, N. Neurite Outgrowths of Neurons with Neurotrophin-Coated Carbon Nanotubes. *J. Biosci. Bioeng.* **2007**, *103*, 216–220.
- (32) Luo, X.; Weaver, C. L.; Zhou, D. D.; Greenberg, R.; Cui, X. T. Highly Stable Carbon Nanotube Doped Poly(3,4-Ethylenedioxythiophene) for Chronic Neural Stimulation. *Biomaterials* **2011**, *32*, 5551–5557.
- (33) Abidian, M. R.; Ludwig, K. A.; Marzullo, T. C.; Martin, D. C.; Kipke, D. R. Interfacing Conducting Polymer Nanotubes with the Central Nervous System: Chronic Neural Recording Using Poly(3,4-Ethylenedioxythiophene) Nanotubes. *Adv. Mater.* **2009**, *21*, 3764–3770.
- (34) Alegret, N.; Dominguez-Alfaro, A.; González-Domínguez, J. M.; Arnaiz, B.; Cossío, U.; Bosi, S.; Vázquez, E.; Ramos-Cabrera, P.; Mecerreyes, D.; Prato, M. Three-Dimensional Conductive Scaffolds as Neural Prostheses Based on Carbon Nanotubes and Polypyrrole. *ACS Appl. Mater. Interfaces* **2018**, *10*, 43904–43914.
- (35) Lovat, V.; Pantarotto, D.; Lagostena, L.; Cacciari, B.; Grandolfo, M.; Righi, M.; Spalluto, G.; Prato, M.; Ballerini, L. Carbon Nanotube Substrates Boost Neuronal Electrical Signaling. *Nano Lett.* **2005**, *5*, 1107–1110.
- (36) Bosi, S.; Rauti, R.; Laishram, J.; Turco, A.; Lonardoni, D.; Nieus, T.; Prato, M.; Scaini, D.; Ballerini, L. From 2D to 3D: Novel Nanostructured Scaffolds to Investigate Signalling in Reconstructed Neuronal Networks. *Sci. Rep.* **2015**, *5*, 9562.
- (37) Jang, M. J.; Namgung, S.; Hong, S.; Nam, Y. Directional Neurite Growth Using Carbon Nanotube Patterned Substrates as a Biomimetic Cue. *Nanotechnology* **2010**, *21*, 235102–235108.
- (38) Bahr, J. L.; Tour, J. M. Highly Functionalized Carbon Nanotubes Using *In Situ* Generated Diazonium Compounds. *Chem. Mater.* **2001**, *13*, 3823–3824.
- (39) Bahr, J. L.; Yang, J.; Kosynkin, D. V.; Bronikowski, M. J.; Smalley, R. E.; Tour, J. M. Functionalization of Carbon Nanotubes by Electrochemical Reduction of Aryl Diazonium Salts: A Bucky Paper Electrode. *J. Am. Chem. Soc.* **2001**, *123*, 6536–6542.
- (40) Barrejón, M.; Syrgiannis, Z.; Burian, M.; Bosi, S.; Fornasiero, P.; Amenitsch, H.; Prato, M. Cross-Linked Carbon Nanotube Adsorbents for Water Treatment: Tuning the Sorption Capacity through Chemical Functionalization. *ACS Appl. Mater. Interfaces* **2019**, *11*, 12920–12930.
- (41) Dyke, A.; Stewart, M. P.; Maya, F.; Tour, J. M. Diazonium-Based Functionalization of Carbon Nanotubes: XPS and GC–MS Analysis and Mechanistic Implications. *Synlett* **2004**, 155–160.
- (42) Schirowski, M.; Tyborsky, C.; Janina, M.; Hauke, F.; Hirsch, A.; Goelcn, J. Reductive Diazotization of Carbon Nanotubes: An Experimental and Theoretical Selectivity Study. *Chem. Sci.* **2019**, *10*, 706–717.
- (43) Maeda, Y.; Saito, K.; Akamatsu, N.; Chiba, Y.; Ohno, S.; Okui, Y.; Yamada, M.; Hasegawa, T.; Kako, M.; Akasaka, T. Analysis of Functionalization Degree of Single-Walled Carbon Nanotubes Having Various Substituents. *J. Am. Chem. Soc.* **2012**, *134*, 18101–18108.
- (44) van der Pauw, L. J. A Method of Measuring the Resistivity and Hall Coefficient on Lamellae of Arbitrary Shape. *Phys. Technol. Rev.* **1958**, *20*, 220–224.
- (45) Cellot, G.; Toma, F. M.; Kasap Varley, Z.; Laishram, J.; Villari, A.; Quintana, M.; Cipollone, S.; Prato, M.; Ballerini, L. Carbon Nanotube Scaffolds Tune Synaptic Strength in Cultured Neural Circuits: Novel Frontiers in Nanomaterial-Tissue Interactions. *J. Neurosci.* **2011**, *31*, 12945–12953.
- (46) Caceres, A.; Banker, G.; Binder, L. Immunocytochemical Localization of Tubulin and Protein 2 During the Development of Hippocampal Neurons in Culture. *J. Neurosci.* **1986**, *6*, 714–722.

- (47) Willmott, N. J.; Wong, K.; Strong, A. J. Intercellular Ca^{2+} Waves in Rat Hippocampal Slice and Dissociated Glial ^ Neuron Cultures Mediated by Nitric Oxide. *FEBS Lett.* **2000**, *487*, 239–247.
- (48) Marconi, E.; Nieuws, T.; Maccione, A.; Valente, P.; Simi, A.; Messa, M.; Dante, S.; Baldelli, P.; Berdondini, L.; Benfenati, F. Emergent Functional Properties of Neuronal Networks with Controlled Topology. *PLoS One* **2012**, *7*, No. e34648.
- (49) Ross, W. N.; Hole, W. Understanding Calcium Waves and Sparks in Central Neurons. *Nat. Rev. Neurosci.* **2015**, *13*, 157–168.
- (50) Grienberger, C.; Konnerth, A. Primer Imaging Calcium in Neurons. *Neuron* **2012**, *73*, 862–885.
- (51) Galante, M.; Nistri, A.; Ballerini, L. Opposite Changes in Synaptic Activity of Organotypic Rat Spinal Cord Cultures after Chronic Block of AMPA/kainate or Glycine and GABA A Receptors. *J. Physiol.* **2000**, *523*, 639–651.
- (52) Rauti, R.; Lozano, N.; León, V.; Scaini, D.; Musto, M.; Rago, I.; Paolo, F.; Severino, U.; Fabbro, A.; Vázquez, E.; Kostarelos, K.; Prato, M.; Ballerini, L. Graphene Oxide Nanosheets Reshape Synaptic Function in Cultured Brain Networks. *ACS Nano* **2016**, *10*, 4459–4471.
- (53) Stetter, O.; Battaglia, D.; Soriano, J.; Geisel, T. Model-Free Reconstruction of Excitatory Neuronal Connectivity from Calcium Imaging Signals. *PLoS Comput. Biol.* **2012**, *8*, No. e1002653.
- (54) Fabbro, A.; Pastore, B.; Nistri, A.; Ballerini, L. Activity-Independent Intracellular Ca^{2+} Oscillations Are Spontaneously Generated by Ventral Spinal Neurons during Development *In Vitro*. *Cell Calcium* **2007**, *41*, 317–329.
- (55) Sokal, D. M.; Mason, R.; Parker, T. L. Multi-Neuronal Recordings Reveal a Differential Effect of Thapsigargin on Bicuculline- or Gabazine-Induced Epileptiform Excitability in Rat Hippocampal Neuronal Networks. *Neuropharmacology* **2000**, *39*, 2408–2417.
- (56) Tibau, E.; Valencia, M.; Soriano, J. Identification of Neuronal Network Properties from the Spectral Analysis of Calcium Imaging Signals in Neuronal Cultures. *Front. Neural Circuits* **2013**, *7*, 1–16.
- (57) Mazzatenta, A.; Giugliano, M.; Campidelli, S.; Gambazzi, L.; Businaro, L.; Markram, H.; Prato, M.; Ballerini, L. Interfacing Neurons with Carbon Nanotubes: Electrical Signal Transfer and Synaptic Stimulation in Cultured Brain Circuits. *J. Neurosci.* **2007**, *27*, 6931–6936.
- (58) Schmidt, C. E.; Shastri, V. R.; Vacanti, J. P.; Anger, R. O. L. Stimulation of Neurite Outgrowth Using an Electrically. *Proc. Natl. Acad. Sci. U. S. A.* **1997**, *94*, 8948–8953.
- (59) Aguado, F.; Carmona, M. A.; Pozas, E.; Aguiló, A.; Martínez-guijarro, F. J.; Alcantara, S.; Borrell, V.; Yuste, R.; Ibañez, C. F.; Soriano, E. BDNF Regulates Spontaneous Correlated Activity at Early Developmental Stages by Increasing Synaptogenesis and Expression of the K^+/Cl^- Co-Transporter KCC2. *Development* **2003**, *130*, 1267–1280.
- (60) Yang, L.; Qi, Y.; Yang, Y. Astrocytes Control Food Intake by Inhibiting AGRP Neuron Activity via Adenosine A_1 Receptors. *Cell Rep.* **2015**, *11*, 798–807.
- (61) Marom, S.; Shahaf, G. Development, Learning and Memory in Large Random Networks of Cortical Neurons: Lessons beyond Anatomy. *Q. Rev. Biophys.* **2002**, *35*, 63–87.
- (62) Arosio, D.; Ratto, G. M. Twenty Years of Fluorescence Imaging of Intracellular Chloride. *Front. Cell. Neurosci.* **2014**, *8*, 258.
- (63) Martín, C.; Merino, S.; González-Domínguez, J. M.; Rauti, R.; Ballerini, L.; Prato, M.; Vázquez, E. Graphene Improves the Biocompatibility of Polyacrylamide Hydrogels: 3D Polymeric Scaffolds for Neuronal Growth. *Sci. Rep.* **2017**, *7*, 10942.